Cornucopian Cylindrical Aggregate Morphologies from Self-Assembly of Amphiphilic Triblock Copolymer in Selective Media

Ying Jiang,[†,‡] Jintao Zhu,[§] Wei Jiang,*[,§] and Haojun Liang*[,†,‡,§]

Hefei National Laboratory for Physical Sciences at Microscale, University of Science & Technology of China, Hefei, Anhui, 230026, People's Republic of China, Department of Polymer Science and Engineering, University of Science & Technology of China, Hefei, Anhui, 230026, People's Republic of China, State Key Laboratory of Polymer Physics and Chemistry, Changchun Institute of Applied Chemistry, Chinese Academy of Sciences, Changchun 130022, and Graduate School of the Chinese Academy of Sciences, People's Republic of China

Received: May 10, 2005; In Final Form: July 18, 2005

We have investigated, both experimentally and theoretically, the aggregation of ABA amphiphilic triblock copolymers in dilute solution. We observed a number of complex architectures having toroidal and network structures, including some novel ones. The computational analyses of these systems offer some insight into the origins of the self-assembly of these amphiphiles. The results we obtained using real-space self-consistent field theory reveal that the formation of network and toroidal structures from the block copolymers occurs as the result of the breaking of "inhomogeneous vesicles"; the observed polymorphism results from the existence of multiple metastable states.

1. Introduction

Nanoscale aggregation through the self-assembly of block copolymers in selective solvents is the subject of an extensive number of investigations because of their industrial potential for applications in many fields, including drug delivery, cosmetics, catalysis, separations, microelectronics, and materials.[1−9] Amphiphilic block copolymers have been demonstrated to possess the ability to self-assemble in solution into various complex ordered microstructures, such as spherical micelles, rodlike micelles, large compound micelles, vesicles, large compound vesicles, hexagonally packed hollow hoop structures ("HHH" structures), and tube-, onion-, and bowl-shaped structures.[10−16] Among these complex microstructures, the branched, network, and toroidal micelles have attracted the most attention.[17−19] Bates and co-workers demonstrated that the diblock copolymer poly(1,2-butadiene-*b*-ethylene oxide) (PB-PEO) can self-assemble into Y-junctions and three-dimensional networks, which formed through the re-assembly of the Y-junctions.[17] Very recently, Pochan and co-workers found that almost all of the microstructures assembled from poly(acrylic acid-*b*-methyl acrylate-*b*-styrene) (PAA_{99}-PMA_{73}-PS_{66}) triblock copolymers are ringlike or toroidal micelles.[19] If we attribute toroid formation to the re-assembly of Y-junctions, we should find Y-junctions in the equilibrium structures, as did Bates and co-workers in their system, but Y-junctions are rarely found (cf. the images in refs 18 and 19). Therefore, these experimental results verified that the toroidal aggregates might not form through an end-to-end connection process, which implies the existence of other mechanisms for the formation of the micro-structures in dilute solution. In addition, another feature shared by the assembly of block copolymers in dilute solution is the coexistence of disparate morphologies, i.e., very different patterns coexist in solution.[6,7] The reason for the coexistence of those disparate morphologies, i.e., polymorphism, remains an open problem. With these problems in mind, we studied the aggregation morphologies of the P4VP-*b*-PS-*b*-P4VP triblock copolymer in dilute solution and then used self-consistent field theory (SCFT) under similar conditions to those used experimentally in an effort to provide some new insight into the process.

2. Experimental Section

2.1. Sample Preparation. The copolymer used in this study was the triblock copolymer $P4VP_{43}$-*b*-PS_{260}-*b*-$P4VP_{43}$ (the subscripts indicate the block lengths; PDI = 1.09), which was purchased from Polymer Source Inc., Canada. The indirect method was used to prepare sample 1. The triblock copolymer was first dissolved in dioxane (initial concentration ranged from 0.5 to 4 wt %), which is a good solvent for both the PS and P4VP blocks, and then deionized water was added, at a rate of 0.2 wt %/min to the copolymer solution up to 25 wt %, with stirring to induce the self-assembly of the block copolymer. The resulting solution was then stirred for 1 day. Subsequently, the solution was sealed and kept for 15 days without stirring. Finally, a large amount of deionized water was added to the solution to quench the resulting aggregates. The resulting mixture was dialyzed against distilled water to remove dioxane from the solution.

For sample 2, a direct sample preparation method was used. The block copolymer was dissolved in a dioxane/water mixture (initial copolymer concentration in the common solvent was 1 wt %) having a water content of 25 wt %. The solution was then stirred for different periods of time. Finally, a large amount water was added, and dialysis was performed. The length of time between the dissolution of the copolymer into the solvent mixture and the addition of the large amount water was

* Authors to whom correspondence should be addressed. E-mail: hjliang@ustc.edu.cn (H.J.L.); wjiang@ciac.jl.cn (W.J.).

† Hefei National Laboratory for Physical Sciences at Microscale, University of Science and Technology of China.

‡ Department of Polymer Science and Engineering, University of Science and Technology of China.

§ State Key Laboratory of Polymer Physics and Chemistry, Changchun Institute of Applied Chemistry, Graduate School of the Chinese Academy of Sciences.

10.1021/jp052420m CCC: $30.25
Published on Web 10/20/2005

considered to be the annealing time. During all of the dialysis processes, the pH of the distilled water was adjusted to 4 to prevent the colloid solutions from precipitating. [7, 18]

2.2. Transmission Electron Microscopy. The resulting aggregate morphologies were visualized using a combination of a regular transmission electron microscope (TEM) and a tapping-mode atomic force microscope (AFM). Transmission electron microscopy was performed using a JEOL JEM-2000FX TEM operating at an acceleration voltage of 160 kV. The dialyzed colloidal solutions were diluted by a factor of 10−20 to prepare the TEM samples. A drop of the very dilute solution was placed onto a copper TEM grid covered with a polymer support film that had been precoated with thin film of carbon. After 15 min, the excess of the solution was blotted away using a strip of filter paper. The samples were left to dry in air and at room temperature for 1 day before observation.

2.3. Atomic Force Microscopy. An SPA300HV AFM was operated in the tapping mode using an SPI3800 controller (Seiko instruments Industry Co., Ltd.). The tip was of a sharpened tetrahedral type (R < 10 nm; tip height: 14 μm) and the cantilever fabricated from silicon had a spring constant of 2 N/m and a resonance frequency of 70 kHz. To prepare the samples for AFM, the very dilute solution (a few drops) obtained after dialysis was spin-coated onto the freshly cleaved mica substrates. All of the samples were dried in air at room temperature for 1 day prior to observation. The AFM experiments were all performed in air and at room temperature.

3. Theoretical Section

In this section, we outline the formulation of self-consistent field theory (SCFT) for analyzing **ABA** amphiphilic triblock copolymers in dilution solution. Amphiphlic triblock copolymers having hydrophilic segments (**A**), hydrophobic segments (**B**), and solvent molecules (**S**) are involved in a volume V. The volume fractions of segments **A** and **B** in the system are f_A and f_B, respectively. As a result, the volume fractions of the copolymer and solvent in solution are $f_P = f_A + f_B$ and $f_S = 1 - f_P$, respectively. In real-space SCFT, one considers the statistics of a single copolymer chain in a set of effective chemical potential fields ω_I, where the subscript I represents a block species, either **A** or **B**. Those chemical potential fields, which replace the actual interactions between the different components, are conjugated with the segment density field, ϕ_I, of the block species I. Similarly, the solvent molecules are considered to be in an effective chemical potential field ω_S that conjugates with the solvent density field ϕ_S. Hence, the free energy function (in units of k_BT) of the system is given as follows:

$$F = -f_S \ln(Q_S/V) - \frac{f_P}{N}\ln(Q_P/V) + \frac{1}{V}\int \mathrm{d}r[\chi_{AB}\phi_A\phi_B + \chi_{AS}\phi_A\phi_S + \chi_{BS}\phi_B\phi_S - \omega_A\phi_A - \omega_B\phi_B - \omega_S\phi_S - P(1 - \phi_A - \phi_B - \phi_S)] \quad (1)$$

where N is the length of the copolymer chain, χ_{ij} is the Flory−Huggins interaction parameter between species i and j, P is the Lagrange multiplier (as a pressure), $Q_S = \int \mathrm{d}r \exp(-\omega_S)$ is the partition function of the solvent in the effective chemical potential field ω_S, and $Q_P = \int \mathrm{d}r q(r, 1)$ is the partition function of a single chain in the effective chemical potential field ω_A or ω_B. The end-segment distribution function $q(r, s)$ provides the probability that a section of a chain, having contour length s and containing a free chain end, has its "connected end" located at r. The parametrization is chosen such that the contour variable s increases continuously from 0 to 1, corresponding from one end of the chain to the other. With the use of a flexible Gaussian chain model to describe the single-chain statistics, the function $q(r, s)$ satisfies the following modified diffusion equation:

$$\frac{\partial}{\partial s}q(r, s) = \nabla^2 q(r, s) - N\theta_i(s)\omega_i q(r, s) \qquad (i = 1, 2, 3) \quad (2)$$

where $\theta_i(s)$ is equal to 1 if s belongs to block i; otherwise it is equal to 0. In eq 2, the lengths are scaled by the (overall) radius of gyration of an unperturbed chain. The appropriate initial condition is $q(r, 0) = 1$. Here, ω_i is ω_A when $0 < s < f_1$ and $f_1 + f_2 < s < 1$ or ω_B when $f_1 < s < f_1 + f_2$ (f_i is the volume fraction of block i). Similarly, the second distribution function $q'(r, s)$ (containing another chain end) is also satisfied by eq 2 with the initial condition $q'(r, 0) = 1$, but in this case, ω_i is ω_A when $0 < s < f_3$ and $f_2 + f_3 < s < 1$ or ω_B when $f_3 < s < f_2 + f_3$. The density of each component is obtained by using the equation

$$\phi_{A(B)}(r) = \frac{1}{Q_P}\int_0^1 \mathrm{d}s q(r, s)q'(r, 1 - s)\theta_i(s) \quad (3)$$

$$\phi_S(r) = \frac{\exp(-\omega_S(r))}{Q_S}$$

From the equilibrium condition, the minimization of free energy with respect to density and pressure, $\delta F/\delta\phi = \delta F/\delta P = 0$, we obtain another four equations:

$$\begin{aligned}
\omega_A(r) &= \chi_{AB}(\phi_B(r) - f_B) + \chi_{SA}(\phi_S(r) - f_S) + P(r)\\
\omega_B(r) &= \chi_{AB}(\phi_A(r) - f_A) + \chi_{BS}(\phi_S(r) - f_S) + P(r)\\
\omega_S(r) &= \chi_{SA}(\phi_A(r) - f_A) + \chi_{BS}(\phi_B(r) - f_B) + P(r)\\
\phi_A(r) &+ \phi_B(r) + \phi_S(r) = 1
\end{aligned} \quad (4)$$

Here, constant shifts in the potential are introduced into the equations.

Using this method allows the low free-energy solutions of the equations to be determined within a planar square or box having a periodic boundary condition. The initial value of ω is constructed as $\omega_j(r) = \Sigma_{i\neq j}\chi_{ij}(\phi_i(r) - f_i)$, where f_i represents the average volume fraction of the copolymer segments or solvent and $\phi_i(r) - f_i$ satisfies the Gaussian distributions:

$$\begin{aligned}
\langle(\phi_i(r) - f_i)\rangle &= 0\\
\langle(\phi_i(r) - f_i)\,(\phi_j(r') - f_j)\rangle &= \beta f_i f_j \delta_{ij}\delta(r - r')
\end{aligned} \quad (5)$$

Here, β is defined as the density fluctuation at the initial temperature. The effective pressure field, $P = C_2C_3(\omega_A + \omega_B) + C_1C_3(\omega_B + \omega_S) + C_1C_2(\omega_A + \omega_S)/2(C_1C_2 + C_2C_3 + C_1C_3)$, on each grid is obtained upon solving eq 4, where $C_1 = \chi_{SA} + \chi_{BS} - \chi_{AB}$, $C_2 = \chi_{SA} + \chi_{AB} - \chi_{BS}$, and $C_3 = \chi_{AB} + \chi_{BS} - \chi_{SA}$. The density field ϕ_I of species I, conjugated with the chemical potential field ω_I, can be evaluated based on eqs 2 and 3. The chemical potential field ω_I can be updated by using the equation $\omega_I^{new} = \omega_I^{old} + \Delta t(\delta F/\delta\phi_I)^*$, where $(\delta F/\delta\phi_I)^* = \sum_{M\neq I}\chi_{IM}(\phi_M(r) - f_M) + P(r) - \omega_I^{old}$ is the chemical potential force. In our simulation, the time step was $\Delta t = 0.3$, and we iterated the above steps until the free energy converged to a local minimum where the phase structure corresponds to a metastable state. This iteration scheme constitutes a pseudo-dynamic process having the steepest descent on the energy

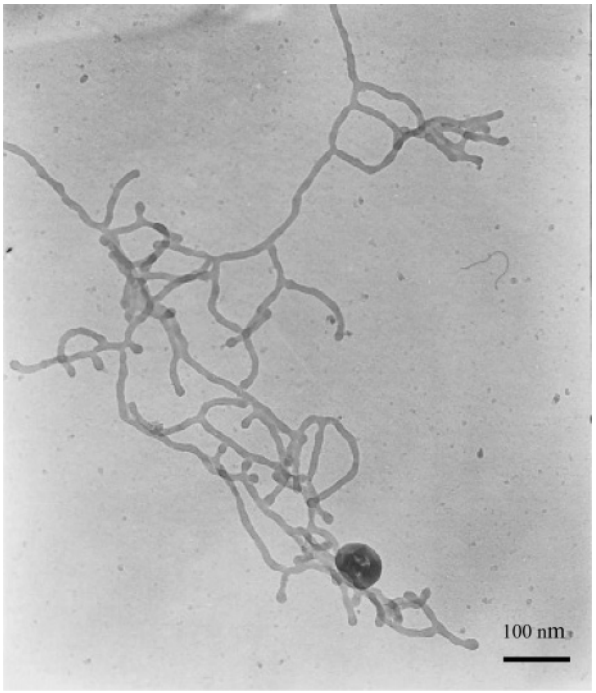

Figure 1. TEM micrograph of a sample prepared using the indirect method, displaying part of the network formed from 4 wt % P4VP(43)-*b*-PS(260)-*b*-P4VP(43) in a dioxane/water mixture having a water content of 25 wt %.

landscape by being nearest to the metastable solution. It is possible to reach various metastable states, depending on the initial conditions.

We performed the numerical simulation on the three-dimensional space using a $40 \times 40 \times 40$ cubic lattice having space $L = 13.333$ and grid size $\Delta x = 0.3333$ in the units of R_g (unperturbed mean-square radius of gyration of a copolymer chain). The simulation for each sample was performed until the phase pattern was stable and invariable with time and $\Delta F < 10^{-6}$. The simulation of the homogeneous block copolymer solution was reiterated for 10 to ca. 20 times from different initial random states and using different random numbers to ensure that the phenomena were not accidental. In the present simulation, the length of chain N was 68, the length fraction of the **A** block was 0.147, and f_P was 0.1 to ensure that the system reflected a dilute solution. We assumed the interaction parameters to be $\chi_{AB}N = 25.5$, $\chi_{BS}N = 27.2$, and $\chi_{AS}N = -15.3$, respectively; these values ensure that the long middle block (B block) is hydrophobic and the two end blocks (A blocks) are hydrophilic, to be consistent with the experimental results. In particular, we considered **ABA** triblocks that were symmetric about their midpoint, i.e., the **A** blocks are fixed at an equal length (equal volume fractions $f_1 = f_3$).

4. Results and Discussion

Figure 1 displays the results of using the indirect method (sample 1) to determine the three-dimensional branched aggregates of 4 wt % $P4VP_{43}$-*b*-PS_{260}-*b*-$P4VP_{43}$ (abbreviated as ABA) in a dioxane/water mixture containing 25 wt % water. The branches are unambiguously distinguishable from the overlaps through measurement of the optical densities at the junctions, i.e., the overlaps appear darker than other parts of the micelles, while the optical densities are uniform throughout the branches. The branched cylinders can also be clearly observed from the AFM height images (in Figure 2 the arrows point at the branches). We found that the aggregate morphologies were sensitive to the initial copolymer concentration in dioxane. The aggregates comprised stretched (or individual) rods and only occasionally did we observe branches when the copolymer concentration was 1 wt % in dioxane. The experimental results indicate that branch formation was favored at a higher copolymer concentration. From the TEM and AFM images (Figures 1 and 2), we can readily identify many 3-fold interconnecting cylindrical micelles (Y-junctions terminated by enlarged spherical caps), resulting in a network. Moreover, the occasional looped structure can be observed in the structure, and the enlarged end-caps can also be seen clearly at the ends of the stretched rodlike microstructures. Therefore, both branched linear wormlike micelles and Y-junctions terminated by enlarged spherical caps characterize this representative image. Similarly, Kindt and Tlusty et al. predicted theoretically that, under appropriate conditions, Y-junctions would appear in cylinder-forming three-component (surfactant/oil/water) microemulsions, leading to network formation and phase separation.[21−23] Rods interconnected in three dimensions are also observed occasionally through experiment. The diameters of the rods are monodisperse, and the origin of the branched points is the same as that of the bicontinuous morphology observed in the bulk. The Eisenberg group reported a similar result that they observed from polystyrene-*b*-poly(acrylic acid)/DMF/water systems.[24−26] It has been proposed that the formation of the interconnected rods must occur mainly as a result of adhesive collisions and fusion of the micelles.

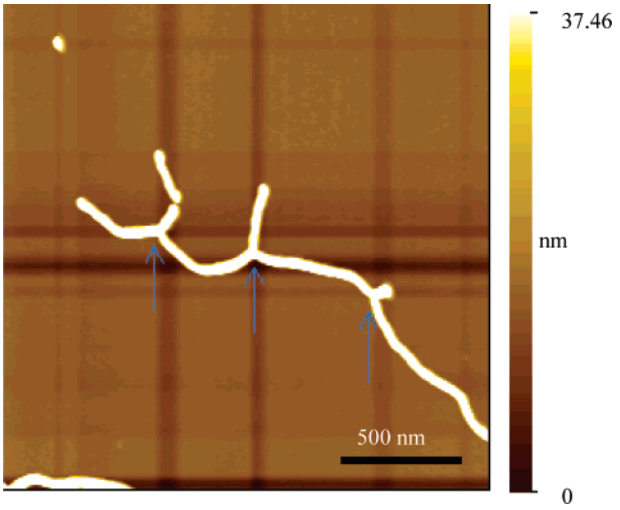

Figure 2. AFM height images of the branched cylindrical aggregate formed from the copolymer/dioxane/water mixture presented in Figure 1.

Figure 3 displays the results of using the direct method, a typical TEM micrograph, of the aggregate morphologies of 1 wt % triblock copolymer in a dioxane/water mixture containing 25 wt % water. In addition, we also observe complex looped micelles in the AFM height images presented in Figure 4 (see the arrows). The micrograph is characterized by a mixture of looped micelles and network-like compound micelles. Very few Y-junctions were terminated by enlarged spherical caps relative to those found in Figures 1 and 2 and ref 17. The difference between Figures 1 and 3 suggests that the micellar morphologies are critically dependent on the choice of manufacturing process. It can be understood that the structures in dilute solution, which should correspond to a set of metastable states, closely relate to the initial states and the manufacturing conditions.

At present, there are only a few theoretical reports on studies of the formation of these types of complex microstructures.[21−23] On the basis of the results published by Kindt[21] and Tlusty et

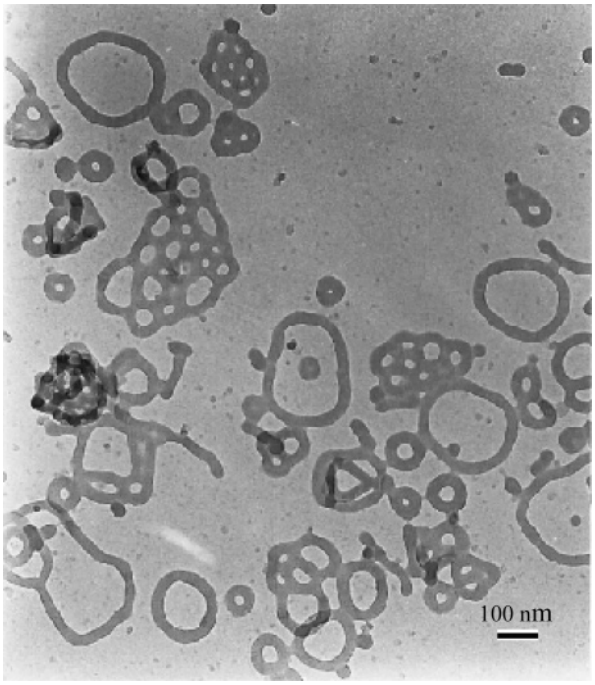

Figure 3. TEM micrographs of a sample prepared using the direct method, displaying the aggregates formed from 1 wt % P4VP(43)-*b*-PS(260)-*b*-P4VP(43) in a dioxane/water mixture, having a water content of 25 wt %, after annealing for 6 days.

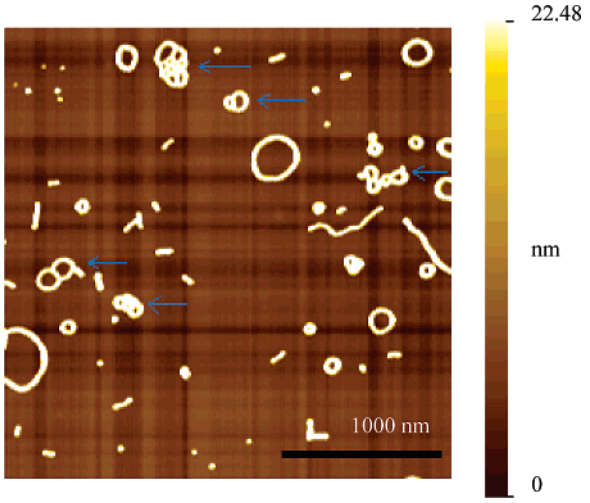

Figure 4. AFM height images of the ramification (see the arrow) formed from 1 wt % P4VP(43)-*b*-PS(260)-*b*-P4VP(43) in a dioxane/water mixture, having a water content of 25 wt %, after annealing for 6 days (i.e., the sample presented in Figure 3).

al.,[22,23] a possible mechanism for the formation of the toroid or network in Figure 3 might be that initially wormlike micelles having Y-junctions terminated with enlarged spherical caps are generated and then these micelles convert into toroidal micelles through intrafusion of the ends of the worms; finally, these toroidal and wormlike micelles fuse together and rearrange into network compound micelles. If this mechanism is correct, the Y-junctions should be favored over the toroidal micelles so that it would be reasonable to expect that the wormlike micelles and Y-junctions terminated with enlarged spherical caps should be visible among the final microstructures, as was observed by the Eisenberg group in their system.[24−26] The Y-junctions terminated with enlarged spherical caps that were observed in ref 17 and in Figures 1 and 2 are, however, rarely observed in our Figure 3. The dominating microstructures in Figure 3 are the compound toroidal and individual toroidal micelles. These differences might imply a different mechanism for the formation of these microstructures, i.e., other mechanisms may exist besides the one suggested by Kindt and Tlusty et al. To clarify the matter, we applied the self-consistent field theory (SCFT) to this system.

SCFT is a mesoscopic simulation technique proposed by Edwards in the 1960s; in subsequent decades, it was adapted explicitly by Helfand and others to treat the self-assembly of block copolymers in melt.[27−31] To circumvent the flaw in the Matsen−Schick approach,[32,33] which requires an initial guess of the relevant morphologies, Drolet and Fredrickson suggested the implementation of a real-space SCFT where low free-energy morphologies are obtained upon relaxation from random potential fields.[34−36] Recently, Liang and co-workers applied the method to the investigation of the mesophases (e.g., sphere- and wormlike micelles or vesicles) of amphiphilic diblock copolymers in dilute solution.[37] Herein, we use this approach to study the toroid and network formation that occurs upon the self-assembly of the triblock copolymers in dilute solution.

Figure 5 displays the network, looped, wormlike, and spherical micelles obtained through both simulation and experiment. It is clear that some of the typical microstructures observed experimentally were reproduced in the simulations. The initial component density in the simulations satisfies the Gaussian distribution expressed as

$$\langle(\phi_i(\mathbf{r}) - f_i)\rangle = 0$$

$$\langle(\phi_i(\mathbf{r}) - f_i)(\phi_j(\mathbf{r}') - f_j)\rangle = \beta f_i f_j \delta_{ij}\delta(\mathbf{r} - \mathbf{r}')$$

(i, j runs all of the components)

where $\phi_i(\mathbf{r})$ represents the respective component density at $\mathbf{r}$, f_i is the average density of the different components, and β is defined as the initial density fluctuation amplitude. An observation of the toroid formation process depicted in Figure 5D reveals that the triblock copolymers initially aggregated into an "inhomogeneous vesicle," a micelle whose water and hydrophilic components are distributed inhomogeneously within its center. Upon growing to a critical size, this inhomogeneous vesicle breaks at a certain place on the surface; this process leads to the redistribution of the block copolymers as a result of the balance of the internal free energy. As a result, a toroidal structure is produced (Figure 5D). A detailed description of the evolution of this process is described in a following section.

Figure 6a displays the evolution of a single loop. From the results of the simulation, we find that the early stages of this microstructure's formation are quite similar to that observed the case of the vesicle. During the first 50 steps [Figure 6a (I)], the solvent in the irregular micelle is absolutely dominant [Figure 6b (I-S)] and the hydrophilic segment A [Figure 6b (I-A)] and hydrophobic block B [Figure 6b (I-B)] are dispersed homogeneously in the micelle. After 100 steps [Figure 6a (II) and (III)], the density of the hydrophilic block A in the central area of the irregular micelle increases gradually [Figure 6b (II-A), (III-A)] as a result of the attractive force of the solvent. Simultaneously, Figure 6b (II-B) and (III-B) indicates that the density of the hydrophobic block B increases around the central area of the hydrophilic block A. The existence of hydrophobic segment B leads to a decrease in the solvent density in that region because of repulsion between the hydrophobic segment and the solvent. Because of the inhomogeneous distribution of the hydrophobic block B around the central area of the hydrophilic block A, the polymeric shell comprised of block B begins to break [Figure 6b (III-B)]. Subsequently, a connection

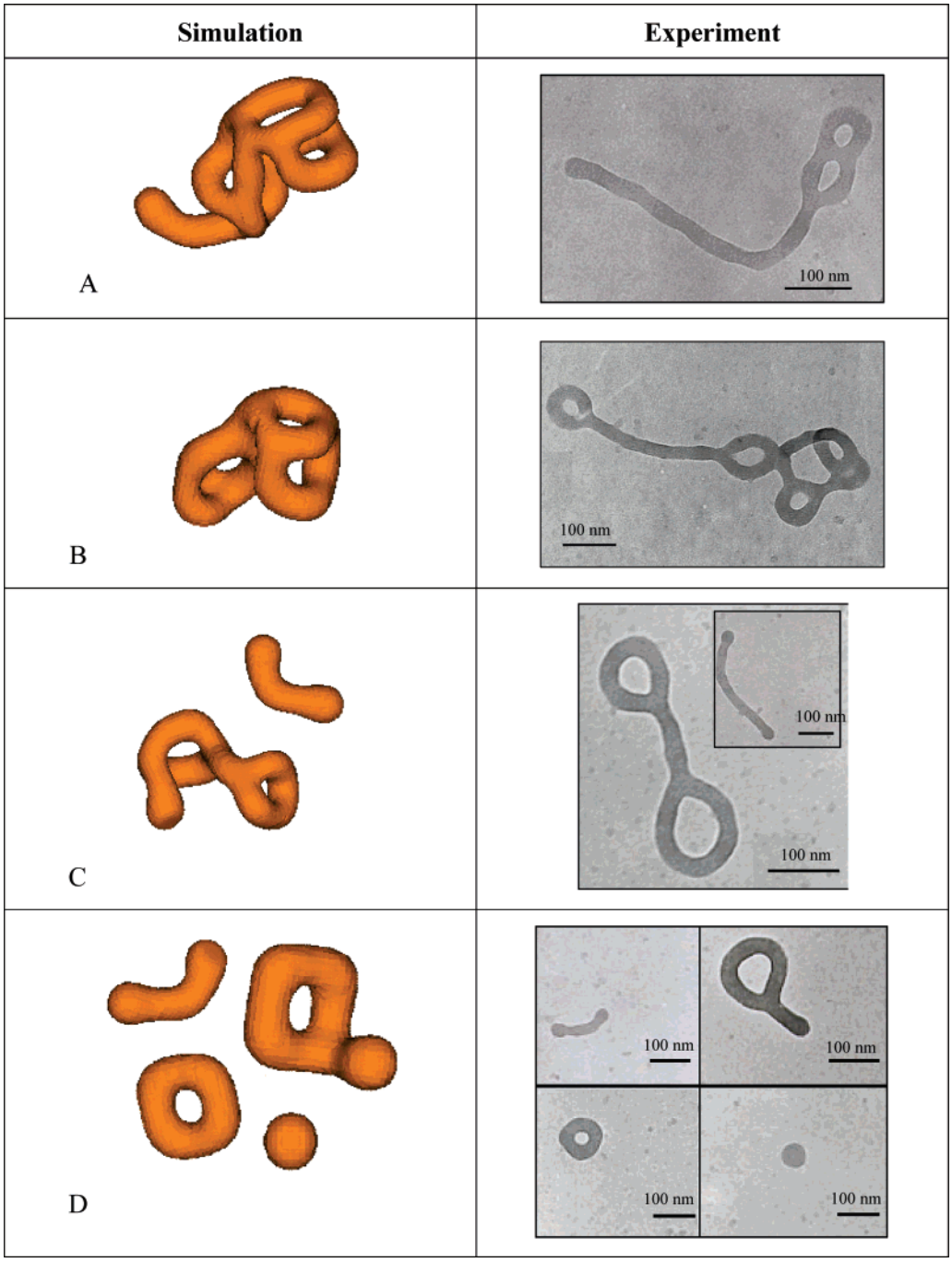

Figure 5. Ordered microphases of the amphiphilic triblock copolymer in dilute solution obtained at different values of the initial density fluctuation β and relative free energy F ($\Delta F < 10^{-6}$ in our calculations) and using the interaction parameters $\chi_{AB}N = 25.5$, $\chi_{BS}N = 27.2$, and $\chi_{AS}N = -15.3$; (A) $\beta = 1.0 \times 10^{-6}$, $F = 0.8203$; (B) $\beta = 2.5 \times 10^{-5}$, $F = 0.8182$; (C) $\beta = 2.5 \times 10^{-3}$, $F = 0.8245$; (D) $\beta = 0.01$, $F = 0.8374$. For the sake of comparison, TEM micrographs of the samples prepared experimentally using the direct method are presented in the right-hand column.

is formed between the solvent molecules within and outside the irregular micelle [Figure 6b (IV-S)]. As noted upon processing from I to III, the volumes for those three micelles are nearly the same [Figure 6a (I), (II), and (III)]. We presume that the triblock copolymer chains diffuse outside into the early-formed irregular micelle, which helps the assembly of the micelle. Next, the connectivity between the solvents inside and outside the micelle leads to the redistribution of components A and B. As noted in Figure 6b IV, the density of the hydrophobic component in the central area decreases in this area, while that of the hydrophilic component increases. In particular, we note that the hydrophilic component became homogeneously distributed in the central area during the following evolution process, as indicated in Figure 6b (V-A). It is the hydrophilic component in the central area that attracts the solvent into this region. Finally, upon further evolution, the solvent dissolved a circular hole to form a single cylindrical loop (Figure 6a VI) in which the solvent occupies the center completely (Figure 6b VI-S).

The double loops or network microstructures in the three other groups depicted in Figure 5A−C are formed through similar processes, but they broke in more than one place on the surface. Figures 7 and 8 display some of the typical subpatterns that appeared in the numerous samples prepared using the direct method. A striking feature shared by all of the micelles presented in these figures is their mirror symmetry, which reflects the

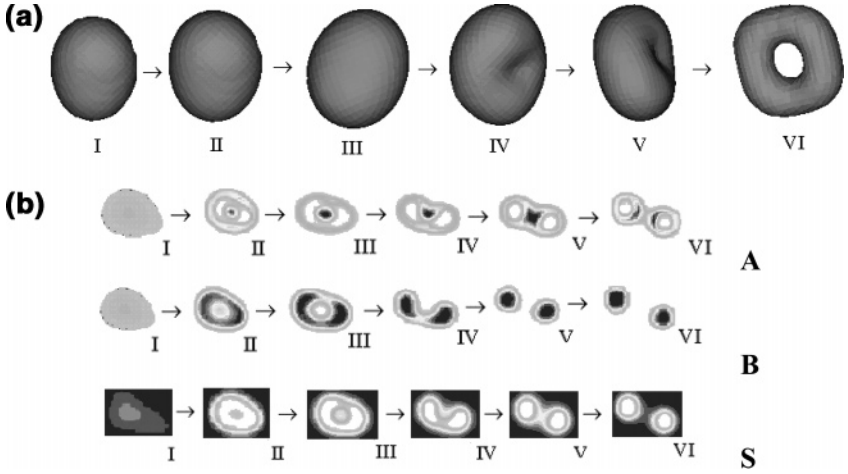

Figure 6. (a) Ordered microphases (from Figure 5D) of the amphiphilic triblock copolymer in dilute solution at different times during its evolution: (I) $t = 15$; (II) $t = 30$; (III) $t = 150$; (IV) $t = 300$; (V) $t = 375$; (VI) equilibrium state. (b) Isodense density distributions (ϕ) of **A**, **B**, and **S** along the cross-section of the diameter of the terminally formed loop presented in Figure 5D, but perpendicular to the plate on which the loop resides, calculated at different times during its evolution. Black indicates high density; gray, low density.

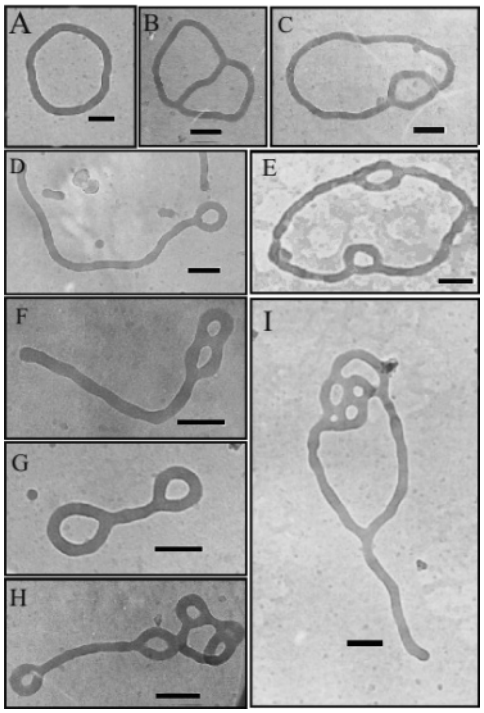

Figure 7. Typical TEM micrographs of a sample prepared using the direct method, depicting the complex looped structures most often observed from 1 wt % P4VP(43)-*b*-PS(260)-*b*-P4VP(43) in a dioxane/water mixture after annealing for different periods of time (bar length: 100 nm).

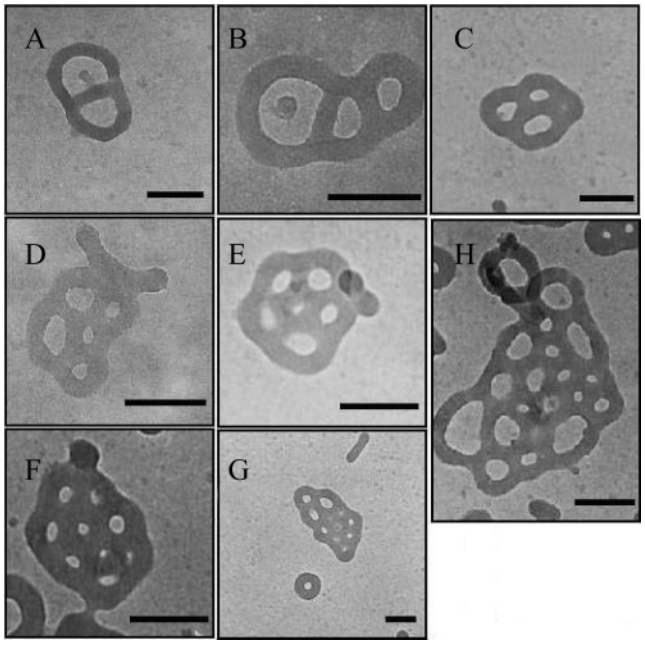

Figure 8. Typical TEM micrographs of a sample prepared using the direct method, depicting the looped ramification most often observed from 1 wt % P4VP(43)-*b*-PS(260)-*b*-P4VP(43) in a dioxane/water mixture after annealing for different periods of time (bar length: 100 nm).

tendency to balance the internal free energy through the redistribution, by fragmentation, of the block copolymer molecules after micelle formation.[17] Herein, we provide a mechanism that is different from the one suggested by Kindt and Tlusty et al. The aggregation of the triblock copolymer in dilute solution is a complex process, and thus, it is reasonable that more than one mechanism may exist to govern the process.

Another remarkable feature disclosed by the TEM images (cf. Figure 3) of the polymeric aggregates is the coexistence of disparate morphologies, i.e., the network and the multiple, double, and single loops possessing tails all coexist in Figures 3, 7, and 8. This polymorphism is generally found in other polymeric aggregate systems in dilute solution.[20,38] It has been proposed that the polydispersity inherent in macromolecular samples is one factor that, at least partially, contributes to this coexistence,[36] but such polymorphism is far from understood. It is a worthwhile task to perform further theoretical studies. As stated above, the aggregate structures of the block copolymer chains in dilute solution are dependent on the initial density fluctuation amplitude β. In fact, a solution that is homogeneous on the macroscale can be inhomogeneous on the microscale. For instance, the local density of polymer chains will be different from region to region. Thus, once phase separation occurs, those pre-aggregated chains arising from density fluctuation should act as "nuclei" from which the phase growth begins. Because of the β dependence of the final microstructures, fluctuations having a smaller or larger amplitude will lead to a variety of diverse morphologies. Certainly, in applications of real-space SCFT to concentrated solutions and melts, β dependence of the microstructures was not found because the initial density fluctuation amplitude was very small relative to the original density, i.e., its influence was negligible (note that the coexist-

ence of diverse morphologies is seldom observed in melts). In the cases when using dilute solutions, however, the initial density fluctuation amplitude was comparable to its original density, and its influence could no longer be ignored. The values of β and the free energies obtained from the simulations in Figure 5 are (A) $\beta = 1.0 \times 10^{-6}$, $F = 0.8203$; (B) $\beta = 2.5 \times 10^{5}$, $F = 0.8182$; (C) $\beta = 2.5 \times 10^{-3}$, $F = 0.8245$; and (D) $\beta = 0.01$, $F = 0.8374$, respectively. Obviously, each system does not possess the lowest free energy, but rather is trapped in higher free-energy states, i.e., in a set of metastable states. Again, from these data, we observe that the structures depend so sensitively on the β values that a tiny change in β may result in quite different morphologies. We believe that inhomogeneity in solution can definitely lead to the coexistence of these disparate morphologies. This concept explains, at least partially, why the diverse micromorphologies for a given block copolymer in dilute solution can be produced experimentally through different manipulation procedures. Thus, we attribute the polymorphism of this system largely to its metastability, in addition to the polydispersity of the triblock copolymer. Our results are similar to those observed in vesicle systems formed through the self-assembly of $P4VP_{43}$-*b*-PS_{366}-*b*-$P4VP_{43}$ in dilute solution.[39] The preparation of these metastable states depends strongly on which path the system travels on the free-energy landscapes; these routes are governed by the initial conditions, such as the local density fluctuations.

5. Conclusions

We have obtained cornucopian aggregates, including some novel structures, from an ABA amphiphilic triblock copolymer in selective media. These complex morphologies enrich our knowledge of the potential products obtained from the self-assembly of block copolymers in selective media, and they offer us some insight into the self-assembly process. The results of simulations performed using the SCFT reveal that the formation of network and looped structures from the block copolymers is due to the breaking of "inhomogeneous vesicles." A main reason for the coexistence of the diverse morphologies in dilute solution is that the systems exist in a set of metastable states that correlate well with the initial density fluctuation (β). Filtration of these branched and looped cylindrical aggregates should yield highly porous layers that we believe could have significant practical interest. Porous solids of this type might be attractive as supports for immobilized enzymes (or other catalysts) and for applications such as chromatography or sewage separation, where stability, a large hydrophilic surface area, and easy accessibility to liquids are all necessary properties.[40] Moreover, these branched and network structures may offer new opportunities for designing advanced materials having defined properties.

Acknowledgment. We are grateful for the financial support provided by the General (203074050, 90403022) and Major (20490220) Programs of the National Natural Science Foundation of China (NSFC), the Chinese Academy of Sciences (project KJCX2-SW-H07), the 973 Program of MOST (nos. 2005CB623807, 2003CB615600), and the Fund for Distinguished Youth of Jilin Province, China.

References and Notes

(1) Beck, J. S.; Vartuli, J. C.; Roth, W. J.; Leonowicz, M. E.; Kresge, C. T.; Schmitt, K. D.; Chu, C. T. W.; Olson, D. H.; Sheppard, E. W. *J. Am. Chem. Soc.* **1992**, *114*, 10834.
(2) Savic, R.; Luo, L.; Eisenberg, A.; Maysinger, D. *Science* **2003**, *300*, 615.
(3) Yang, H.; Coombs, N.; Sokolov, I.; Ozin, G. A. *Nature* **1996**, *381*, 589.
(4) Qi, L.; Li, J.; Ma, J. *Adv. Mater.* **2002**, *14*, 300.
(5) Jenekhe, S. A.; Chen, L. *Science* **1998**, *279*, 1903.
(6) Disher, D. E.; Eisenberg, A.; *Science* **2002**, *297*, 967.
(7) Shen, H. W.; Zhang, L. F.; Eisenberg, A. *J. Am. Chem. Soc.* **1999**, *121*, 2728.
(8) Lu, B.; Li, X.; Scriven, L. E.; Davis, H. T.; Talmon, Y.; Zakin, J. L. *Langmuir* **1998**, *14*, 8.
(9) Föster, S.; Antonietti, M. *Adv. Mater.* **1998**, *10*, 195.
(10) Shen, H.; Eisenberg, A. *Angew. Chem., Int. Ed.* **2000**, *39*, 3310.
(11) Gohy, J. F.; Willet, N.; Varshney, S.; Zhang, J. X.; Jérôme, R. *Angew. Chem., Int. Ed.* **2001**, *40*, 3214.
(12) Cameron, N. S.; Corbierre, M. K.; Eisenberg, A. *Can. J. Chem.* **1999**, *77*, 1311.
(13) Yu, K.; Eisenberg, A. *Macromolecules* **1996**, *29*, 6359.
(14) Zhang, L. F.; Bartele, C.; Yu, Y.; Shen, H. W.; Eisenberg, A. *Phys. Rev. Lett.* **1997**, *79*, 503.
(15) Talingting, M. R.; Munk, P.; Webber, S. E. *Macromolecules* **1999**, *32*, 1593.
(16) Lazzari, M.; López-Quintela, M. A. *Adv. Mater.* **2003**, *15*, 1583.
(17) Jain, S.; Bates, F. S. *Science* **2003**, *300*, 460.
(18) Zhu, J. T.; Liao, Y. G.; Jiang, W. *Langmuir* **2004**, *20*, 3809.
(19) Pochan, D. J.; Chen, Z. Y.; Cui, H. G.; Hales, K.; Qi, K.; Wooley, K. L. *Science* **2004**, *306*, 94.
(20) Won, Y. Y.; Brannan, A. K.; Davis, H. T.; Bates, F. S. *J. Phys. Chem. B* **2002**, *106*, 3354.
(21) Kindt, J. T. *J. Phys. Chem. B* **2002**, *106*, 8223.
(22) Tlusty, T.; Safran, S. A. *Science* **2000**, *290*, 1328.
(23) Tlusty, T.; Safran, S. A.; Strey, R. *Phys. Rev. Lett.* **2000**, *84*, 1244.
(24) Yu, K.; Zhang, L. F.; Eisenberg, A. *Langmuir* **1996**, *12*, 5980.
(25) Zhang, L. F.; Eisenberg, A. *J. Polym. Sci., Part B: Polym. Phys.* **1999**, *37*, 1469.
(26) Zhang, L. F.; Eisenberg, A. *Macromolecules* **1999**, *32*, 2239.
(27) Edwards, S. F. *Proc. Phys. Soc., London* **1965**, *85*, 613.
(28) Helfand, E. *J. Chem. Phys.* **1975**, *62*, 999.
(29) Helfand, E.; Wasserman, Z. R. *Macromolecules* **1976**, *9*, 879.
(30) Hong, K. M.; Noolandi, J. *Macromolecules* **1981**, *14*, 727.
(31) Vavasour, J. D.; Whitmore, M. D. *Macromolecules* **1992**, *25*, 5477.
(32) Matsen, M. W.; Schick, M. *Phys. Rev. Lett.* **1994**, *72*, 2660.
(33) Matsen, M. W. *J. Chem. Phys.* **1998**, *108*, 785.
(34) Drolet, F.; Fredrickson, G. H. *Phys. Rev. Lett.* **1999**, *83*, 4317.
(35) Drolet, F.; Fredrickson, G. H. *Macromolecules* **2001**, *34*, 5317.
(36) Fredrickson, C. H.; Ganesan, V.; Drolet, F. *Macromolecules* **2002**, *35*, 16.
(37) He, H. X.; Liang, H. J.; Huang, L.; Pan, C. Y. *J. Phys. Chem. B* **2004**, *108*, 1731.
(38) Zhang, L. F.; Eisenberg, A. *Polym. Adv. Technol.* **1998**, *9*, 677.
(39) Won, Y. Y.; Brannan, A. K.; Davis, H. T.; Bates, F. S. *J. Phys. Chem. B* **2002**, *106*, 354.
(40) Zhu, J. T.; Jiang, Y.; Liang, H. J.; Jiang, W. *J. Phys. Chem. B* **2005**, *109*, 8619.
(41) Yu, K.; Zhang, L. F.; Eisenberg, A. *Langmuir* **1996**, *12*, 5980.